International Journal of Dynamics and Control (2018) 6:1175–1182
https://doi.org/10.1007/s40435-017-0378-7

High-precision microfluidic pressure control through modulation of dual fluidic resistances

Michael J. Toth[1] · Tomohiro Kawahara[2] · YongTae Kim[1,3,4,5]

Received: 18 July 2017 / Revised: 9 October 2017 / Accepted: 15 November 2017 / Published online: 4 December 2017

Abstract
This work presents an approach to the modulation of dual fluidic resistances for long-term, high-speed, and high precision (less than 0.5% steady-state error) control of the inlet pressure of a microfluidic device. This is accomplished through independent controls of dual variable resistances in a fluid network between a pressurized reservoir and a microfluidic device. We show the superior characteristics of the system with dual resistance modulation by experimentally comparing our new model with our previous approach. We demonstrate the performance of the controlled system and address the long-term stability and robustness. This system can be utilized in a variety of applications that require high-precision, high-speed, and long-term controls of microfluidic flows, including chemical synthesis, cell sorting, energy harvesting optofluidics, microbial fuel cells, and multiscale biological investigation of cellular or tissue level.

Keywords Pressure control · Fluidic resistance · Nonlinear · Feedback control · Microfluidics

1 Introduction

Microfluidic technologies have developed for a broad range of applications including life sciences [1,2], chemistry [3,4], energy conversion [5,6], and defense [7]. These technologies are reliant on syringe pumps, open-loop based control, to exploit laminar fluid flow, resulting in non-robust control of flow rates with the inability to address disturbances such as unpredictable pressure variation from desirable pressure values in microfluidic devices [8]. Syringe pumps exhibit long setting times, upwards of minutes [9,10], for low flow rates (μL/min) within microfluidic channels, due to high fluidic resistances, on the order of 1E+15 Pa · s/m^3. At these low flow rates, syringe pumps have been shown to develop fluctuating flow, due to the stepper motor mediated disturbances [11,12], a potentially damaging problem for flow sensitive systems.

To overcome the inability of syringe pumps to mitigate external disturbances, various approaches have been proposed by decreasing system sensitivity [13,14] or implementing feedback control on syringe pumps with pressure/flow sensors [15–18]. Alternatively, to syringe pumps, pressure feedback control systems, which relate pressure to flow through the Hagan–Poiseuille equation, have been developed [19,20]. These pressure systems overcome limitations of syringe pumps by removing the mechanical fluidic driving mechanism, and allowing for a constant pressure source. Additionally, the expandable reservoir of pressure control systems eliminates the reliance on a finite syringe volume. Recent development of high-precision pressure control technology in microfluidics has yielded commercially available products.

We also previously developed a pressure modulation mechanism using a variable resistance and a variable reservoir in a fluidic network to allow long-term (duration of 15 h) and high-speed (setting time less than 0.5s) control of

✉ YongTae Kim
ytkim@gatech.edu

Michael J. Toth
mtoth6@gatech.edu

Tomohiro Kawahara
kawahara@lsse.kyutech.ac.jp

1 George W. Woodruff School of Mechanical Engineering, Georgia Institute of Technology, Atlanta, GA 30332, USA

2 Department of Biological Functions Engineering, Kyushu Institute of Technology, Kitakyushu 808-0196, Japan

3 Wallace H. Coulter Department of Biomedical Engineering, Georgia Institute of Technology, Atlanta, GA 30332, USA

4 Parker H. Petit Institute for Bioengineering and Bioscience, Georgia Institute of Technology, Atlanta, GA 30332, USA

5 Institute for Electronics and Nanotechnology, Georgia Institute of Technology, Atlanta, GA 30332, USA

microfluidic flows [21,22]. We developed a nonlinear model, based on fluidic circuit analog [23], controlled by a designed compensator-integrator, demonstrating precision fluid control in microfluidics. We demonstrated the variable reservoir allows for rapid fluidic drainage, decreasing the inlet pressure, and improves the settling time of the pressure response by over 500%, compared to a single variable resistor only model. The finite volume of the variable reservoir potentially limits the flexibility of controller performance, by limiting fluidic drainage.

In this brief, we develop an enhanced nonlinear pressure modulation mechanism system that is based on independent controls of dual fluidic resistances for long-term, high-speed, and high-precision (less than 0.5% steady-state error) control of the inlet pressure in microfluidic devices. Instead of using a single DC motor applied in our previous model [21,22], we use dual linear actuators to achieve independent modulation of dual fluidic resistances, which provides versatile controller design and implementation. Through continuous and discrete time models (SIMULINK®) of the nonlinear pressure modulation mechanism, we predict and tune a linear controller for the system. With the tuned controller, we experimentally demonstrate the performance of the controlled system and address long-term stability of this advanced model.

2 Nonlinear modeling

The pressure control system (Fig. 1a) consists of two independent variable resistances, u_{R_1} and u_{R_2}, to control the inlet pressure of a microfluidic device. In this pressure modulation mechanism, u_{R_1} is decreased and u_{R_2} is increased for an increase in pressure (Fig. 1b), while u_{R_1} is increased and u_{R_2} is decreased for a decrease in pressure (Fig. 1c).

To develop a model of the pressure control system, we developed a fluidic circuit analog (Fig. 2) of the system, consisting of fluidic resistance R, fluidic capacitance C, and two variable fluidic resistances u_{R_1} and u_{R_2}. P_r represents the reference pressure that is applied to the source. R_r represents the fluidic resistance of the connection between the source and u_{R_1}. P represents the pressure at the inlet of a microfluidic channel, which is to be controlled in the model. R_i represents the fluidic resistance of a microfluidic inlet. R_o represents the fluidic resistance of a microfluidic outlet. It was shown in our previous work [21] that the contribution of P_o to the change in P can be neglected if $P_o << P$ when the inlet resistance R_i is on the order 1E+3 greater than R_o. In this model, the total flow q is divided into three flow rates (1).

$$q = q_{u_{R_2}} + q_C + q_{R_i} \tag{1}$$

From the circuit model, we define the individual flow rates for total flow (2), $q_{u_{R_2}}$ (3), q_C (4), and q_{R_i} (5).

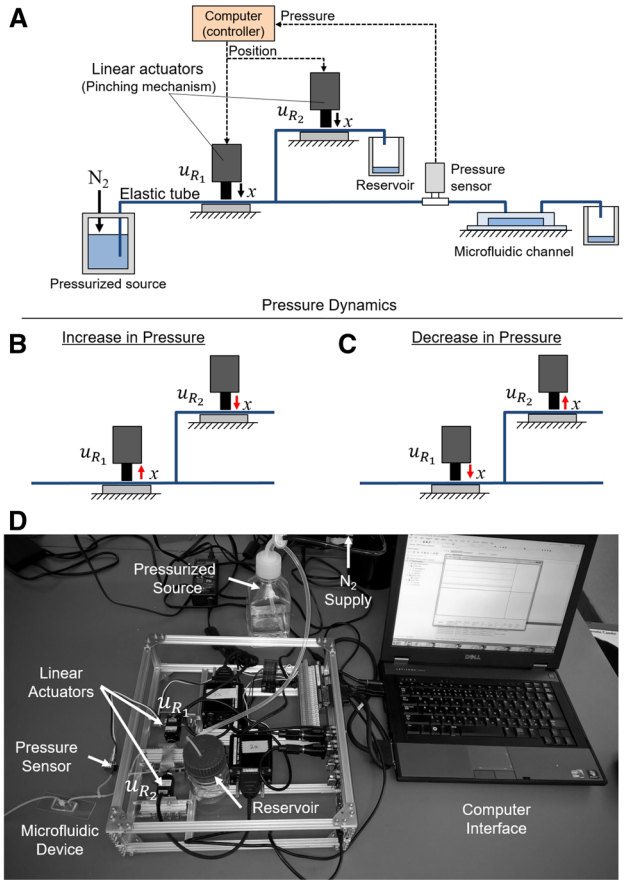

Fig. 1 Pressure control system operation mechanism. Pressure regulation facilitated by the modulation of dual variable resistances, u_{R_1} and u_{R_2}. Linear actuator displacements are regulated by the computer interface in response to the pressure sensor feedback. The displacements of the linear actuator are inversely proportional. **a** Schematic of the pressure control system. **b** Increase and **c** decrease in microfluidic inlet pressure mechanism. **d** Physical control system with computerized interface

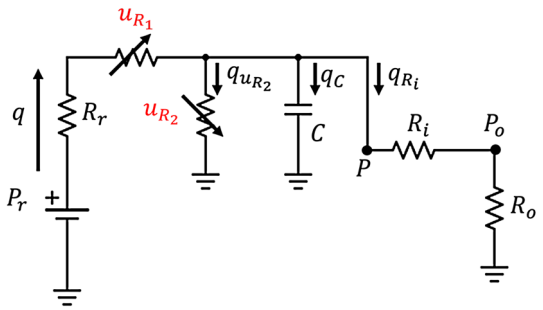

Fig. 2 Fluidic circuit analog decomposition of the pressure control system, represented in Fig. 1a. Pressure control is facilitated by variable resistances u_{R_1} and u_{R_2} (highlighted in red). (Color figure online)

$$q = \frac{P_r - P}{u_{R_1} + R_r} \tag{2}$$

$$q_{u_{R_2}} = \frac{P}{u_{R_2}} \tag{3}$$

$$q_C = \frac{dP}{dt}C \tag{4}$$

$$q_{R_i} = \frac{P}{R_i} \tag{5}$$

From Eqs. (1), (2), (3), (4), and (5), we develop a nonlinear dynamic model for the inlet pressure, P, of the microfluidic device (6).

$$\frac{dP}{dt} = -\left(\frac{1}{\left(u_{R_1} + R_r\right)C} + \frac{1}{R_i C} + \frac{1}{u_{R_2} C}\right)P + \frac{P_r}{(u_{R_1} + R_r)C} \tag{6}$$

This represents a first-order nonlinear differential equation where the time constant can be tuned by modulating the two inputs of the independent resistances u_{R_1} and u_{R_2}. Given that the variable resistances have a lower bound, for a fully released tube, greater than 0, the dynamics of the system can be shown to be stable for all combinations of u_{R_1} and u_{R_2} by examining the equilibrium point (7).

$$P_{eq} = \frac{P_r R_i u_{R_2}}{R_i u_{R_2} + R_i\left(u_{R_1} + R_r\right) + u_{R_2}\left(u_{R_1} + R_r\right)} \tag{7}$$

By perturbing the system away from the equilibrium point by ϵ, where $\epsilon << 1$, we examine rate of change of the pressure, dP/dt. We find that perturbation (8) drives the system back towards the equilibrium point, an indication of stability. This is a result of all variables being positive bounded values.

$$\frac{dP}{dt}(\epsilon) = -\frac{\pm\epsilon\left(\left(R_i + R_r + u_{R_1}\right)u_{R_2} + R_i\left(u_{R_1} + R_r\right)\right)}{u_{R_2} C R_i\left(u_{R_1} + R_r\right)} \tag{8}$$

To complete the model, we incorporate the variable resistance of the tubing into the fluid network. When the linear actuator deforms (compresses or releases) the connective tubing to modify the fluidic resistance, the deformation of the tubing is nonlinear. By assuming a constant inner circumference of the tubing through the deformation, the nonlinearity can be approximated by using weighted averages of both circular and rectangular cross sections; the circular model is accurate near the start of tube compression (i.e. fully released) while the rectangular model is relatively accurate near the end of the tube compression (i.e. fully compressed). To estimate the deformed cross section area of the tubing, we created a model for the full range of the tubing deformation (Fig. 3a). Although an advantage of feedback control is the elimination of the steady-state error allowing for conservative resistance estimations to achieve similar performance; by decreasing the error of the estimation, a more versatile controller can be designed to achieve desired performance.

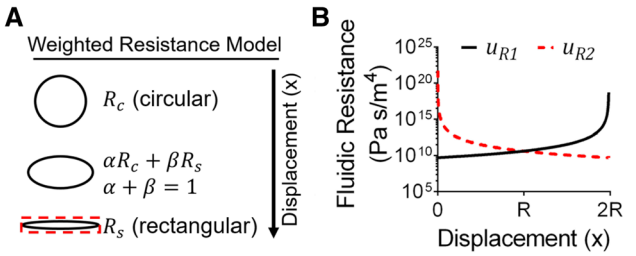

Fig. 3 Modeling and effect of actuator displacement on the resistance u_{R_1} of and u_{R_2}. **a** Weighted average model of circular and square resistances. **b** Simulated fluidic resistance of variable resistors (u_{R_1} and u_{R_2}) along the diameter of the tubing. Radius of the tubing is 3.97E−4 m

The mathematical equation for is modeled as an open tubing (9). Where R represents the original radius of the tubing, μ represents the viscosity of the liquid, L represents the length of compression, and $h(x_1)$ (10) represents the height of the tubing (i.e. the displacement of the linear actuator subtracted from the diameter of the tubing). Similarly, the equation for is modeled as a pinched tubing to reflect the resulting asymmetric motion in the pressure modulation mechanism. The equation for u_{R_2} is obtained by substituting for x_1 using the relationship defined in (11), where α is a proportional scaling constant. Using these equations, the resistance of the tube can be shown as a function of the displacement (Fig. 3b).

$$u_{R_1} = \frac{h(x_1)}{2R}\frac{8\mu L}{\pi\left(\frac{h(x_1)}{2}\right)^4} + \frac{x_1}{2R}\frac{12\mu L}{(\pi R - h(x_1))\,h(x_1)^3\left(1 - \frac{0.630h(x_1)}{\pi R - h(x_1)}\right)} \tag{9}$$

$$h(x_1) = 2R - x_1 \tag{10}$$

$$x_1 = 2R - \alpha x_2 \tag{11}$$

3 Single versus dual resistance model

To compare the contribution of the additional variable resistance for pressure control, we examined a transfer function between the inlet pressure, P, and the linear actuator displacement, x. The transfer function can be derived from the state space matrices through linearization of the differential equation (6). We defined the state space representation with the state variables P, and x with regard to the input u (12)–(15). The state variables P and x were selected, since each state represents a measured value within the system. We obtain P through the pressure sensor feedback and x is measured through the actuator controller. The input of u was chosen as the linear actuator velocity because the physical system requires the movement of the linear actuator (i.e.,

a non-zero velocity profile) to induce a change in variable resistance.

$$\begin{bmatrix} \dot{P} \\ \dot{x} \end{bmatrix} = \begin{bmatrix} F_1 & F_2 \\ 0 & 0 \end{bmatrix} \begin{bmatrix} P \\ x \end{bmatrix} + \begin{bmatrix} 0 \\ 1 \end{bmatrix} u \tag{12}$$

$$F_1 = -\left(\frac{1}{\left(u_{R_1}(x_0) + R_r\right) C} + \frac{1}{R_i C} + \frac{1}{u_{R_2}(x_o)\, C} \right) \tag{13}$$

$$F_2 = \frac{du_{R_1}}{dx}(x_0) \frac{P_r - P_o}{\left(R_r + u_{R_1}(x_0)\right)^2} - \frac{du_{R_2}}{dx}(x_0) \frac{P_o}{u_{R_2}^2(x_0)} \tag{14}$$

$$y = [1\,0] \begin{bmatrix} P \\ x \end{bmatrix} \tag{15}$$

where x_o represents the equilibrium displacement, and P_o represents the equilibrium pressure. By converting the state space model to an equivalent transfer function and expanding out the mathematics, the resulting pressure dynamic transfer function is a type 0 strictly proper transfer function (16). This transformation uses the s-domain differential theorem to convert velocity into displacement, allowing us to define the transfer function between pressure, P, and displacement, x. To observe the benefits of a second variable resistor, we exclude examination of actuator dynamics, which are congruent across each design.

$$G(s) = \frac{\frac{du_{R_1}}{dx}(x_0) \frac{P_r - P_o}{\left(R_r + u_{R_1}(x_0)\right)^2} - \frac{du_{R_2}}{dx}(x_0) \frac{P_o}{u_{R_2}^2(x_0)}}{Cs + \left(\frac{1}{R_i} + \frac{1}{\left(R_r + u_{R_1}(x_0)\right)} + \frac{1}{u_{R_2}(x_0)} \right)} \tag{16}$$

For a single variable resistor model, all the fluidic drainage flows through the microfluidic device (i.e. $q_{u_{R_2}} = 0$; $u_{R_2} = \infty$), with resistance tenfold greater than elastic tubing. The transfer function for the single variable resistance model is simply obtained by letting u_{R_2} approach infinity (i.e. the outlet is closed) in Eq. (16). Utilizing the transfer function (16) we can compute the time constants for the single variable resistance model (SVR; 17) and the dual resistance model (DVR; 18).

$$\tau_{SVR} = \frac{C R_i \left(R_r + u_{R_1}\right)}{R_r + u_{R_1} + R_i} \tag{17}$$

$$\tau_{DVR} = \frac{C R_i \left(R_r + u_{R_1}\right) u_{R_2}}{u_{R_2}\left(R_r + u_{R_1}\right) + R_i u_{R_2} + R_i \left(R_r + u_{R_1}\right)} \tag{18}$$

From these time constant definitions, it can be shown that as u_{R_2} approaches infinity (i.e. the outlet is closed) the dual variable resistance time constant (18) converges to the single variable resistance time constant (17). To show the increase in performance of the dual resistance model, we set the condition of $\tau_{DVR} < \tau_{SVR}$ which can be shown to reduce to (19). Given that each of the values is strictly greater than 0, the inclusion of u_{R_2} always results in a faster system response and remains true for all u_{R_1}.

$$R_i \left(R_r + u_{R_1}\right) > 0 \tag{19}$$

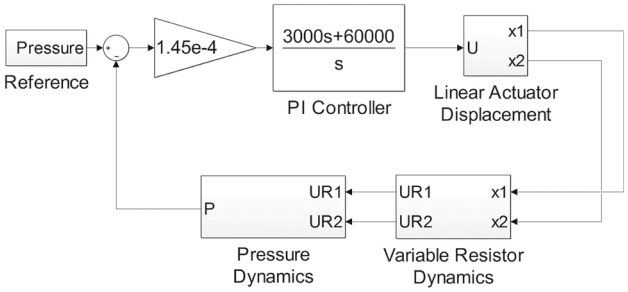

Fig. 4 Coupled continuous model of linear actuator and pressure dynamics

4 Nonlinear simulation and PI controller design

Figure 4 represents the continuous time model of the nonlinear pressure system using SIMULINK®, which consists of a single feedback loop controlled indicative of a pressure sensor. The Linear Actuator Displacement Block converts the controller output to a millimeter displacement while limiting velocity of the actuator to the physical system specifications. The Variable Resistor Dynamics Block utilizes Eqs. (9)–(11) to convert the subsequent displacement to the variable resistance for use in the Pressure Dynamics block, containing the nonlinear pressure dynamics (6).

A PI controller was implemented for the system, to eliminate the steady-state error for a step input, which takes the difference between the reference and pressure response. The traditional gain-tuning approaches including the Ziegler–Nichols method were applied for tuning PID controllers, with which we were able to tune our controller gains to obtain a PI controller that meets the given design specifications. The PI controller was further *ad hoc* tuned to achieved rise time less than 0.3 s while maintaining percent overshoot less than 2%, yielding gains of 3000 and 60,000 for K_p and K_i, respectively. The control effort is applied, after the completion of the loop, to the linear actuator dynamics to calculate the variable resistances for pressure modulation.

To compare the continuous model to a discrete model, we generated a reference pressure set to decrease from 25.1 to 5.1 kPa at 0.5 s; and a pressure increase from 5.1 to 25.1 kPa at 1 s. The response of the continuous system maintains overshoot less than 1.5%, a settling time less than 0.1 s and zero steady-state error, satisfying the design requirements. The similarity between the discrete and the continuous responses

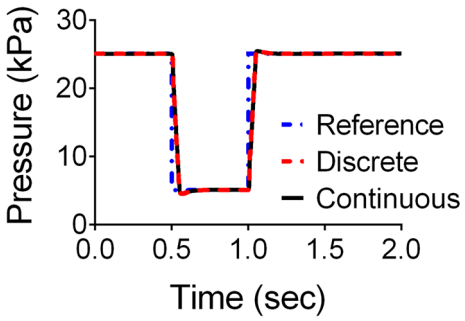

Fig. 5 Simulated response of continuous and discrete pressure dynamic models. Discrete model sampling rate is 1 kHz. (Color figure online)

(Fig. 5) can be attributed to the high sampling rate of the pressure sensor in the discrete time model, 1 kHz, allowing for the reconstruction of the continuous time model. The implementation of the designed gains on the physical system had to be modified to achieve desired performance due to high complexity of the system dynamics not represented in the modeling.

5 Experimental system performance

The system was designed with commercially available electronic components:

- Linear actuator, LAC10A-T4-MC04 (Zaber Technologies, Inc., Vancouver, BC, Canada);
- Stepper Motor Controller, A-MCA-KT05 (Zaber Technologies, Inc., Vancouver, BC, Canada);
- 16-bit AD/DA converter CardBus CSI-360116 (Interface Amita Solutions, Inc., Campbell, CA);
- pressure sensors (ASDX series, Honeywell International Inc., NJ);
- USB-COM232-Plus4 (Future Technology Devices International Ltd, United Kingdom)

These components were connected to a laptop computer via CardBus port. The control software coded by C language was developed and implemented to the laptop computer. The software was composed of two different timer threads; the one for a designed PI controller (sensing and control thread) with 1 ms cycle and the other with 30 ms cycle GUI thread for data drawing and interactive parameter tuning (Fig. 6).

To evaluate the performance of the controlled system, the responses to step and sinusoidal inputs were experimentally evaluated at varying degrees of pressure drops and varying frequencies, respectively, to determine the extent of performance. In these examinations, the response was analyzed from the initiation of reference signal (Fig. 7).

Step responses of pressure drops showed settling times less than 0.3 s with zero steady-state error (Fig. 8). The speed

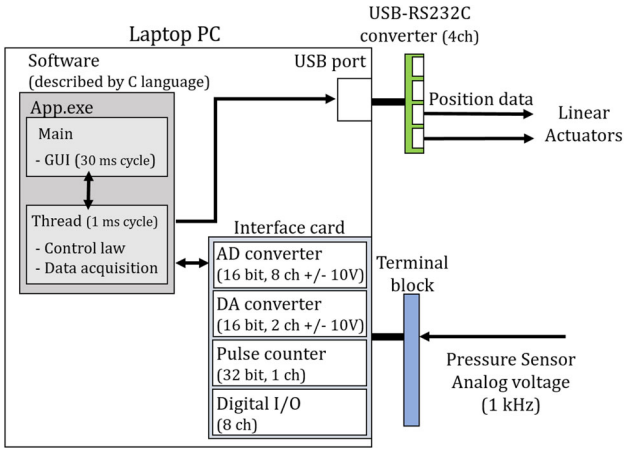

Fig. 6 Pressure controls system computer interface

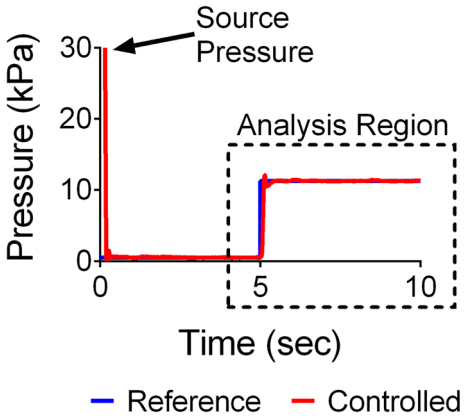

Fig. 7 Definition of analysis region for assessment of experimental pressure system performance. Evaluation of system is at the initiation of the input. (Color figure online)

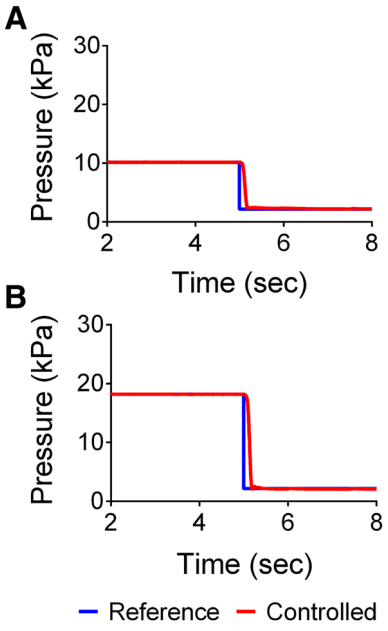

Fig. 8 Experimental response of the pressure control system to pressure drops of **a** 8 and **b** 16 kPa. (Color figure online)

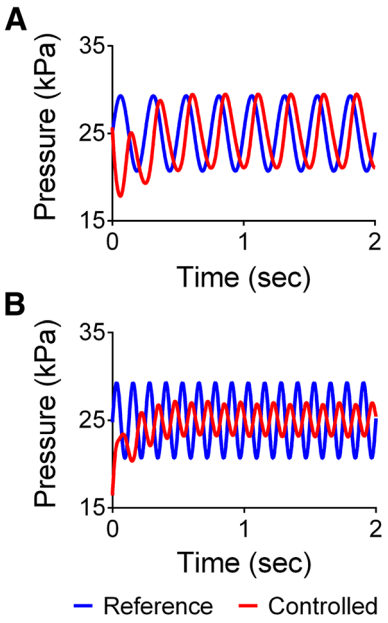

Fig. 9 Experimental response of pressure control system to sinusoidal frequencies of **a** 4 and **b** 8 Hz. (Color figure online)

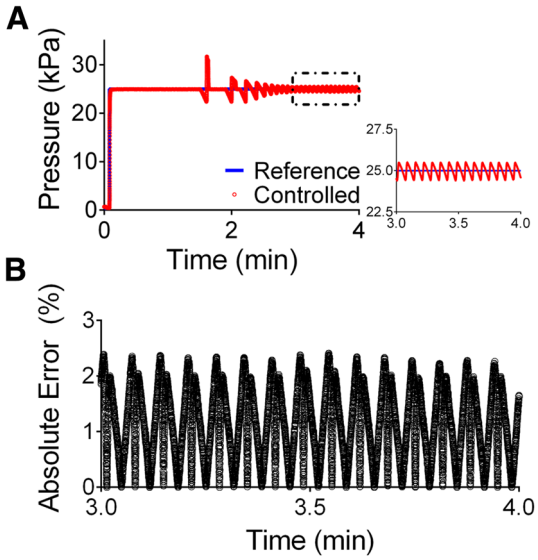

Fig. 10 Experimental evaluation of the variable resistance-variable reservoir model with independent linear actuators with **a** pressure response to a step input and **b** absolute steady-state error. The inset represents steady-state of the induced fluctuation maintained within 2.5%. (Color figure online)

of the decrease is a function of the tube diameter of the reservoir. By allowing a larger diameter tubing, more fluidic drainage can occur leading to sharper decrease in pressure. Although a maximum pressure drop of 16 kPa was demonstrated, by increasing reservoir tube diameter and applying a well-tuned controller, comparable results can be obtained for larger pressure ranges.

The profile of the experimental results matches the simulated results (Fig. 5); however, the settling time of the simulated results remains faster, at less than 0.1 s. This discrepancy between experimentation and simulations can be a function of the unmodeled nonlinearities of the physical system and the change of fluidic inertia. The fluctuation in the steady-state values in these step responses is attributed to factors including external disturbances (e.g. air bubbles in the tubing); rippling of tubing due to high elasticity; and linear actuator perturbations. In addition, the pressure sensor has a 12-bit resolution that may restrict the measurable accuracy. These in combination are contributed to the absolute error at steady-state.

Sinusoidal responses of the pressure control system were observed at 4 and 8 Hz (Fig. 9). It was observed that as the frequency increases ($\geq$ 8 Hz), limited performance in reference following occurs, such as a phase lag and/or a lowered amplitude. Each response can be shown, through the Fast Fourier transform, to match the reference sinusoidal frequency at steady-state. There is a decrease in amplitude, beyond 6 Hz, which can be partially attenuated by increasing the proportional gain; however, remains limited at higher frequencies ($>$ 8 Hz). This limitation results from the limited speed at which the linear actuators can change the resistance and transient response of the fluid to a change in pressure differential. Asymmetric sinusoidal and beat signals can be followed with matching amplitude if the maximum frequency remains below 6 Hz.

6 System comparison

We had previously developed a variable resistance-variable reservoir model for the control of the inlet pressure of the microfluidic device [21]. The variable reservoir provided an alternative fluidic drainage path for rapid decreases in pressure. To observe differences in performance between our dual resistance model and variable resistance-variable reservoir model, we first replaced the mechanically linked operation for adjusting the variable resistor and variable reservoir with the two independent linear actuators. Similar to our dual resistance model, an increase in pressure is facilitated by a decrease the variable resistance, and a compression of the variable reservoir. This compression in turn contributed to an increase in pressure, resulting in an overestimated overshoot of the controlled pressure. Similarly, when the pressure is decreased an undershoot was obtained. Due to this mechanical constraint of the variable resistance-variable reservoir model, a fluctuation developed (Fig. 10a) within 2 min.

To minimize this fluctuation, the variable resistance-variable reservoir model maintains the pressure by either decreasing resistance to the pressure source or by decreasing the volume of the variable reservoir. Particularly, the time

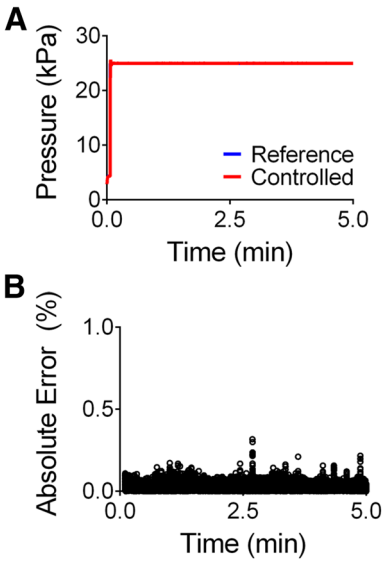

Fig. 11 Experimental evaluation of the dual resistance system with independent linear actuators with **a** long-term pressure response to a step input and **b** absolute steady-state error. (Color figure online)

derivative of volumetric change in the variable reservoir was observed as the primary contributor for high-speed pressure regulation. Once the reservoir is fully compressed by the linear actuator, the pressure can no longer be increased. This causes the pressure to decay until the system responds by decreasing the variable resistance, causing a sharp increase in pressure. This pattern is repeated until the system stabilizes within a percent error of the desired reference signal. Here the PI controller was tuned to achieve an error at stabilization within 2.5% (Fig. 10b), with a root-mean square of the error of 1.361.

By replacing the variable reservoir with a constant outlet, controlled by u_{R_2}, the dual resistance model eliminates the pressure modulation facilitated by the fluidic drainage mechanism. This reduces the overshoot and undershoot observed in the variable resistance-variable reservoir model and eliminates fluctuation during long-term experimentation (Fig. 11a). By examining the absolute steady-state error, we observe an overall reduction of error below 0.5%, with a root-mean square of the error of 0.030 (Fig. 11b).

7 Conclusion

We achieved long-term, high-speed, and high precision (less than 0.5% steady-state error) control of microfluidic pressure using our advanced pressure modulation mechanism (the dual resistance model). The nonlinear models were simulated to validate the use of a 1 kHz sampling rate with no signal loss. A continuous time model simulation was performed to show the performance of a linear controller for the nonlinear model. We developed and tuned a PI controller, enabling the physical system to have a step response reaching the steady-state within 0.3 s within 0.5% steady-state error, experimentally. Using the dual resistance model, we were able to eliminate steady-state fluctuations that were caused by our previous variable resistance-variable reservoir system [21]. This high-precision, high-speed control for long-term experimentation in microfluidic systems can be applied to controlled manufacturing of nanomaterials, which remains a current challenge of syringe-pump based systems. Our dual resistance model system can also be utilized in a variety of areas including biological instrumentation [24,25], organ on a chip [26], chemical gradient manipulation (e.g. controlled drug delivery over a tissue)[27], and chemical synthesis (e.g. nanoparticle synthesis) [28,29].

Acknowledgements This work was supported by the startup resources of Georgia Institute of Technology (Y.K.) and by the National Science Foundation under CAREER CMMI 1653006 (Y.K.).

References

1. Ghaemmaghami AM, Hancock MJ, Harrington H, Kaji H, Khademhosseini A (2012) Biomimetic tissues on a chip for drug discovery. Drug Discov Today 17(3):173–181
2. Kim Y, Langer R (2015) Microfluidics in nanomedicine. Rev Cell Biol Mol Med 1:127–152
3. Song H, Ismagilov RF (2003) Millisecond kinetics on a microfluidic chip using nanoliters of reagents. J Am Chem Soc 125(47):14613–14619
4. Losey MW, Jackman RJ, Firebaugh SL, Schmidt M, Jensen KF (2002) Design and fabrication of microfluidic devices for multiphase mixing and reaction. J Microelectromech Syst 11(6):709–717
5. Mitrovski SM, Elliott LC, Nuzzo RG (2004) Microfluidic devices for energy conversion: planar integration and performance of a passive, fully immersed H_2–O_2 fuel cell. Langmuir 20(17):6974–6976
6. Kim Y, Messner WC, LeDuc PR (2012) Disruptive microfluidics: from life sciences to world health to energy. Disrupt Sci Technol 1(1):41–53
7. Whitesides GM (2006) The origins and the future of microfluidics. Nature 442(7101):368–373
8. Walker GM, Beebe DJ (2002) A passive pumping method for microfluidic devices. Lab Chip 2(3):131–134
9. Stone HA, Stroock AD, Ajdari A (2004) Engineering flows in small devices: microfluidics toward a lab-on-a-chip. Annu Rev Fluid Mech 36:381–411
10. Martin M, Blu G, Eon C, Guiochon G (1975) The use of syringe-type pumps in liquid chromatography in order to achieve a constant flow-rate. J Chromatogr A 112:399–414
11. Li Z, Mak SY, Sauret A, Shum HC (2014) Syringe-pump-induced fluctuation in all-aqueous microfluidic system implications for flow rate accuracy. Lab Chip 14(4):744–749
12. Zeng W, Jacobi I, Beck DJ, Li S, Stone HA (2015) Characterization of syringe-pump-driven induced pressure fluctuations in elastic microchannels. Lab Chip 15(4):1110–1115
13. Lee J, Rahman F, Laoui T, Karnik R (2012) Bubble-induced damping in displacement-driven microfluidic flows. Phys Rev E 86(2):026301

14. Kang YJ, Yang S (2012) Fluidic low pass filter for hydrodynamic flow stabilization in microfluidic environments. Lab Chip 12(10):1881–1889
15. Chien R-L, Parce WJ (2001) Multiport flow-control system for lab-on-a-chip microfluidic devices. Fresenius' J Anal Chem 371(2):106–111
16. Kuczenski B, LeDuc PR, Messner WC (2007) Pressure-driven spatiotemporal control of the laminar flow interface in a microfluidic network. Lab Chip 7(5):647–649
17. Lima JL, Santos JL, Dias AC, Ribeiro MF, Zagatto EA (2004) Multi-pumping flow systems: an automation tool. Talanta 64(5):1091–1098
18. Lake JR, Heyde KC, Ruder WC (2017) Low-cost feedback-controlled syringe pressure pumps for microfluidics applications. PLOS ONE 12(4):e0175089
19. Fütterer C et al (2004) Injection and flow control system for microchannels. Lab Chip 4(4):351–356
20. Lapa RA, Lima JL, Reis BF, Santos JL, Zagatto EA (2002) Multi-pumping in flow analysis: concepts, instrumentation, potentialities. Anal Chim Acta 466(1):125–132
21. Kim Y, LeDuc P, Messner W (2013) Modeling and control of a nonlinear mechanism for high performance microfluidic systems. IEEE Trans Control Syst Technol 21(1):203–211
22. Kim Y, Kuczenski B, LeDuc PR, Messner WC (2009) Modulation of fluidic resistance and capacitance for long-term, high-speed feedback control of a microfluidic interface. Lab Chip 9(17):2603–2609
23. Oh KW, Lee K, Ahn B, Furlani EP (2012) Design of pressure-driven microfluidic networks using electric circuit analogy. Lab Chip 12(3):515–545
24. Kim Y et al (2014) Mechanochemical actuators of embryonic epithelial contractility. Proc Natl Acad Sci 111(40):14366–14371
25. Hovell CM, Sei YJ, Kim Y (2015) Microengineered vascular systems for drug development. J Lab Autom 20:251–258
26. Sei Y, Justus K, LeDuc P, Kim Y (2014) Engineering living systems on chips: from cells to human on chips. Microfluidics Nanofluidics 16(5):907–920
27. Kim Y, Joshi SD, Messner WC, LeDuc PR, Davidson LA (2011) Detection of dynamic spatiotemporal response to periodic chemical stimulation in a Xenopus embryonic tissue. PloS ONE 6(1):e14624
28. Kim Y et al (2013) Single step reconstitution of multifunctional high-density lipoprotein-derived nanomaterials using microfluidics. ACS Nano 7(11):9975–9983
29. Kim Y et al (2012) Mass production and size control of lipid-polymer hybrid nanoparticles through controlled microvortices. Nano Lett. 12(7):3587–3591